Accepted Manuscript

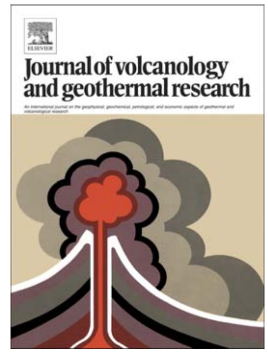

The Masaya Triple Layer: A 2100 year old basaltic multi-episodic Plinian eruption from the Masaya Caldera Complex (Nicaragua)

W. Pérez, A. Freundt, S. Kutterolf, H.-U. Schmincke

PII: S0377-0273(08)00565-9
DOI: doi: 10.1016/j.jvolgeores.2008.10.015
Reference: VOLGEO 4164

To appear in: *Journal of Volcanology and Geothermal Research*

Received date: 9 January 2008
Revised date: 17 September 2008
Accepted date: 16 October 2008

Please cite this article as: Pérez, W., Freundt, A., Kutterolf, S., Schmincke, H.-U., The Masaya Triple Layer: A 2100 year old basaltic multi-episodic Plinian eruption from the Masaya Caldera Complex (Nicaragua), *Journal of Volcanology and Geothermal Research* (2008), doi: 10.1016/j.jvolgeores.2008.10.015

The Masaya Triple Layer: a 2100 year old basaltic multi-episodic Plinian eruption from the Masaya Caldera Complex (Nicaragua)

W. Pérez*, A. Freundt, S. Kutterolf, H.-U. Schmincke
Sonderforschungsbereich (SFB) 574, University of Kiel
IFM-GEOMAR, Wischhofstr. 1-3, 21148 Kiel, Germany

Abstract

The Masaya Caldera Complex has been the site of three highly explosive basaltic eruptions within the last six thousand years. A Plinian eruption ca. 2 ka ago formed the widespread deposits of the Masaya Triple Layer. We distinguish two facies within the Masaya Triple Layer from each other: La Concepción facies to the south and Managua facies to the northwest. These two facies were previously treated as two separated deposits (La Concepción Tephra and the Masaya Triple Layer of Pérez and Freundt, 2006) because of their distinct regional distribution and internal architectures. However, chemical compositions of bulk rock, matrix and inclusion glasses and mineral phases demonstrate that they are the product of a single basaltic magma batch. Additionally, a marker bed containing fluidal-shaped vesicular lapilli allowed us to make a plausible correlation between the two facies, also supported by consistent lateral changes in lithologic structure and composition, thickness and grain size.

We distinguish 10 main subunits of the Masaya Triple Layer (I to X), with bulk volumes ranging between 0.02 and 0.22 km^3, adding up to 0.86 km^3 (0.4 km^3 DRE) for the entire deposit. Distal deposits identified in two cores drilled offshore Nicaragua, at a distance of ~170 km from the Masaya Caldera Complex, increase the total tephra volume to 3.4 km^3 or ~1.8 km^3 DRE of erupted basaltic magma.

Isopleth data of five major fallout subunits indicate mass discharges of 10^6 to 10^8 kg/s and eruption columns of 21 to 32 km height, affected by wind speeds of <2 m/s to ~20 m/s which increased during the course of the multi-episodic eruption. Magmatic Plinian events alternated with phreatoplinian eruptions and phreatomagmatic explosions generating surges that typically preceded breaks in activity. While single eruptive episodes lasted for few hours, the entire eruption probable lasted weeks to months. This is indicated by changes in atmospheric conditions and ash-layer surfaces that had become modified during the breaks in activity. The Masaya Triple Layer has allowed to reconstruct in detail how a basaltic Plinian eruption develops in terms of duration, episodicity, and variable access of external water to the conduit, with implications for volcanic hazard assessment.

Keywords: Masaya Caldera Complex; Nicaragua; basaltic Plinian eruptions; Tephrostratigraphy; Volcanic hazards

* Corresponding author. Tel.: +49 431 6002139; fax: +49 431 6002924
Email address: wperez@ifm-geomar.de

1. Introduction

Plinian eruptions of basaltic composition are thought to be rare because basaltic magma mostly erupts as lava flows and in Strombolian, Hawaiian and Surtseyan fashion when fragmented. Nevertheless, several examples of widely dispersed basaltic tephra deposits with Plinian characteristics have been reported during the last two decades (Williams, 1983; Bice, 1985; Wehrmann et al., 2006; Coltelli et al., 1998; McPhie et al., 1990; Dzurisin et al., 1995; Mastin, 1997; Walker et al., 1984; Sable et al., 2006; Carey et al., 2007; Costantini et al., 2008). The first account of this type of tephra by Williams (1983) addressed two deposits thought to have been erupted from the Masaya Caldera Complex in west-central Nicaragua: the San Judas Formation, later named the Masaya Triple Layer by Bice (1985), and the Fontana Lapilli, later shown by Wehrmann et al. (2006) to have been derived from a vent outside Masaya caldera consistent with its age of ca. 60 ka (Kutterolf et al., 2008a).

Pérez and Freundt (2006) have shown that the Masaya caldera produced three widespread basaltic tephras during the last 6 ka: the San Antonio Tephra, the Masaya Triple Layer, and the Masaya Tuff, a huge hydroclastic surge deposit covered by the Plinian Ticuantepe Lapilli.

Here we reconstruct the ~2.1 ka Plinian eruption of the Masaya caldera which produced the Masaya Triple Layer. We distinguish two facies within the Masaya Triple Layer: La Concepción facies to the south and the Managua facies to the northwest. These two facies were previously treated as two separated deposits (Pérez and Freundt, 2006) because of their distinct regional distribution and internal architectures. However, here we use geochemical and petrographic characteristics to stratigraphically correlate the two facies and to document their origin from a single basaltic magma batch. We reconstruct the evolution of this long-lasting multi-episode eruption based on the revised stratigraphy. Such case studies are needed to better constrain the presently poorly understood processes that force basaltic magmas to erupt in a Plinian fashion.

1.1 Geologic setting

Nicaragua is part of the Central American isthmus, where the subduction of the Cocos plate under the Caribbean Plate at a convergence rate of 70-90 mm/year (Barckhausen et al., 2001; DeMets, 2001) results in the NW-SE trending Central American Volcanic Arc (CAVA). The arc volcanoes lie inside the Nicaraguan depression, which is a NW-SE striking flat depression occupied by Lake Managua and Lake Nicaragua and bordered in the east by the interior highlands (Fig. 1).

The area between the two lakes is the economical and demographic center of the country, where all large cities are located. The capital Managua is surrounded by several highly explosive basaltic to rhyolitic volcanic complexes. Major volcanic threats to the Managua area and its ~1.8 million inhabitants are centered in the Masaya Caldera Complex (Fig. 2), a volcanic system that repeatedly generated highly explosive basaltic eruptions in the past.

The complex consists of a NW-SE elongated caldera 11 km long and 6 km wide, containing Lake Masaya at the SE rim and the post-collapse volcanic edifice in the western half, composed of the Masaya and Nindirí cones with their pit craters Masaya, Santiago, Nindirí and San Pedro (e.g. McBirney, 1956; Rymer et al., 1998). Masaya is one of the most active volcanoes in Central America and has been the object of several geophysical (e.g. Metaxian et al., 1997; Lewicki et al., 2003), gas-chemical (e.g., Stoiber et al., 1986; Horrocks et al., 1999; Duffell et al., 2003) and geochemical (Walker et al., 1993) investigations.

Three widespread pyroclastic deposits that originated at Masaya were previously identified: the Fontana Lapilli, the Masaya Triple Layer or San Judas Formation and the Masaya Tuff or El Retiro Tuff (Bice, 1985; Williams 1983). We have additionally identified the ca. 6 ka old San Antonio Tephra (Pérez and Freundt, 2006). A recent detailed study of the Fontana Tephra by Wehrmann et al. (2006) showed that the source vent of this basaltic Plinian lapilli fallout did not lie within the Masaya caldera as previously interpreted (Williams, 1983) but a few kilometers outside to the NW, where it would be part of the older Las Nubes caldera (Girard and van Wyk de Vries, 2005). The Fontana Tephra age of ~60 ka documented in Kutterolf et al. (2007, 2008a) supports this result. The ~6 ka San Antonio Tephra is thus the oldest known product of a basaltic Plinian eruption from the Masaya caldera.

The second Plinian eruption at Masaya caldera produced the Masaya Triple Layer (Williams, 1983; Bice, 1985). Re-investigation by Pérez and Freundt (2006) identified two basaltic tephra deposits overlying the San Antonio Tephra which differ in regional distribution and internal architecture: the Masaya Triple Layer with a radiocarbon age of 2.1 ka to the NW, and La Concepción Tephra south of the caldera (Fig. 2). These deposits are the subject of this paper. The last large eruption from the Masaya caldera produced the Masaya Tuff, a huge phreatomagmatic pyroclastic surge deposit (Bice, 1985; Williams, 1983). This large-magnitude Surtseyan eruption terminated in a third Plinian eruption that produced the widespread Ticuantepe Lapilli, a stratified succession of well-sorted fallouts of vesicular scoria immediately overlying the Masaya Tuff (Pérez and Freundt, 2006). Kutterolf et al. (2008a) estimated that this eruption occurred 1.8 ka ago, based on stratigraphic relationships in offshore sediment cores. Younger products of Masaya volcanism formed the intra-caldera

Santiago-Masaya volcanic cone and numerous smaller cones and lava flows within, and partly outside the caldera (McBirney, 1956; Williams, 1983; Walker et al., 1993).

1.2 Methodology

Our stratigraphic subdivisions and correlations are based on 108 logged outcrops around the Masaya caldera. Correlations between outcrops are based on lithological criteria as well as compositional data. Tephra volumes are derived from isopachs maps applying the methods of Pyle (1989) and Fierstein and Nathenson (1992). Erupted magma masses were calculated by subtracting the average volume fraction of pores and lithic fragments from the tephra volumes for each subunit, and then multiplying by a density of 2500 kg/m^3. Distal thickness data and isopachs of the total deposit are from marine gravity cores collected offshore Nicaragua during research cruises M54/2, M66/3a (RV METEOR) and SO173/3 (RV SONNE) (Kutterolf et al., 2008a). Geometric measures from isopleth maps, based on the average of the five largest juvenile or lithic clasts, are used to estimate eruption column heights and discharge rates from comparison with model results of Carey and Sparks (1986), Wilson and Walker (1987), Woods (1988) and Sparks et al. (1992).

Bulk rock major and trace element compositions were determined by X-Ray Fluorescence (XRF) analyses carried out at IFM-GEOMAR and Inductively Coupled Plasma Mass Spectrometry (ICP-MS) at the University of Kiel. Mineral, matrix and inclusion glass compositions were determined by electron microprobe at IFM-GEOMAR. Laser Ablation Inductively Coupled Plasma Mass Spectrometry (LA-ICP-MS) at Frankfurt University was used for the trace element chemistry of glass samples.

2. The Masaya Triple Layer

Pérez and Freundt (2006) distinguished two deposits that differ in internal architecture and regional distribution but occur in the same stratigraphic position: La Concepción Tephra to the south of Masaya caldera and Masaya Triple Layer to the northwest and across Managua city (Fig. 2). Here, we re-name these deposits as La Concepción facies and Managua facies, respectively, while applying the name Masaya Triple Layer (MTL) to the entire deposit.

Numerous exposures of MTL exist to the NW and S of Masaya caldera, but no trace was found in the lowlands NE of the caldera although stratigraphically underlying and overlying units do occur, as well as on the mountainous Las Sierras ridge to the SW where strong erosion has removed younger deposits (Fig. 2). The MTL is separated from the underlying San Antonio Tephra by a paleosol and an erosional unconformity. A yellowish massive reworked tuffaceous deposit separates the MTL from the overlying Chiltepe Tephra in the Managua area while the MTL is directly overlain by the Masaya Tuff in the south, with a locally intervening erosional unconformity.

Both facies of the MTL consist of well-sorted black lapilli beds, coarse ash layers and grayish indurated tuffs, some with desiccation cracks at the top. The well-sorted layers consist mostly of juvenile scoria lapilli to coarse-ash and minor (~1-3 vol. %) lithic fragments mainly of basaltic lava and rare gabbro. The scoria fragments vary from highly vesicular (up to 80 vol. % vesicles) to dense juvenile lapilli (<5 vol. % vesicles; using the vesicularity index of Houghton and Wilson, 1989). The matrix of the scoriae varies from sideromelane with abundant round vesicles through dark brown to black tachylite with rare irregularly shaped vesicles (Fig. 3). Phenocrysts are mainly plagioclase with abundant melt inclusions and minor olivine and clinopyroxene; groundmass microlites are plagioclase and olivine. The bulk-rock composition is basaltic (50.2-51 wt% SiO_2 and 3.5-4.0 wt% alkalis; Fig. 4).

2.1 La Concepción facies

La Concepción facies (**LCF**) is composed of 17 layers (B0-B16) of well-sorted scoria lapilli to coarse-ash intercalated with tuffs (Pérez and Freundt, 2006). The upper contact of the deposit is variably eroded. At some localities it is overlain by a thick overburden of a clayey sediment, while at other places it is separated from the Masaya Tuff by a deeply incised erosional unconformity.

Most exposures show the succession from B1 to B11 and part of B12 but only a few outcrops show the complete sequence shown in figure 5. The lowermost layer B0 crops out only in three exposures <6 km south of the caldera rim and consist of two basal fine ash layers and a cemented accretionary lapilli-bearing tuff at the top containing hydrothermally altered lithic clasts and plant remains.

Subunit B5 the thickest lapilli layer of the LCF and most distinctive by being composed of fluidal-textured achnelith lapilli and ash (Fig. 6). Hence it is a useful marker bed in all outcrops. The total thickness of B5 decreases from 115 cm at 1 km south from the vent to 12 cm at 10 km, where it appears as a single thin layer of achnelith-shaped fine lapilli. In proximal sections, where the well-sorted, black lapilli fallout is vaguely stratified by vertically alternating grain size and interrupted by a thin light yellowish layer of fine ash, we distinguish

5 levels from bottom to top: **[a]** a highly vesicular, glassy, faintly laminated, moderately well-sorted lapilli layer with minor amount of juvenile ash and very few lithics. Most of the juvenile fragments have elongated or contorted shapes, **[b]** is a yellowish fine ash layer commonly 1 cm thick but reaching 4 cm at 1 km from the caldera rim. **[c]** is the thickest level reaching 90 cm in the proximal areas. The juvenile particles are similar to [a] but grain size is larger, size-sorting is better particularly at the top, and the content of lithic fragments is slightly higher (~1 vol. %). The base of this layer is weakly stratified and consists of fine lapilli to coarse ash. **[d]** is a weakly stratified medium-ash layer of glassy scoria that is slightly cemented and **[e]** is a scoria lapilli layer similar to [a].

The tuff triplet B6, B8, B10 are also characteristic of the LCF and they thin rapidly southwards away the caldera rim (Fig. 7). The grayish indurated B6 tuff is in proximal exposures composed of a lower fine-grained part with accretionary lapilli and an overlying cross-bedded layer of fine lapilli to coarse ash. In medial exposures, this unit is condensed to an indurated tuff with vesicular lapilli at the bottom and a laminated medium to fine ash layer with scarce accretionary lapilli at the top.

B8 is an indurated tuff up to 60 cm thick at proximal locations (~1 km from the vent). Its lower part is cross-bedded with dune structures of alternating coarse and fine lapilli layers. In the medial facies, B8 is a 20 cm thick tuff with a 1 cm yellowish fine ash at the bottom, overlain by an indurated fine tuff with accretionary lapilli and dispersed glassy scoria clasts. A strongly cemented light gray fine tuff layer forms the top.

B10 is proximally stratified, poorly-sorted, coarse ash with dispersed lapilli at the base, fine to medium ash with dune structures in the middle portion, and a highly indurated tuff at the top. At medial exposures S or SE from the caldera rim, B10 consists of an indurated grayish cross-bedded tuff with coarse ash and fine lapilli at the bottom and a fine ash with accretionary lapilli at the top (Fig. 7). At distal exposures to the S and SW, it appears as a thin indurated tuff with accretionary lapilli, slightly laminated at the bottom.

2.2 Managua facies

The Managua facies of the MTL north and northwest of the caldera consists of 10 layers (C1 to C10), 7 of them are scoria lapilli to coarse-ash layers and the others are tuffs (Fig. 8, table 2). No outcrops could be found close to the Masaya caldera rim, the most proximal are those located at 7 to 7.5 km distance, along the road from San Antonio Sur to El Crucero, where the facies reaches its maximum observed thickness. Here we describe four characteristic layers of the MF, brief descriptions of all subunits are given in table 2.

Layer C2 is a well-sorted fine lapilli layer of highly vesicular scoria containing <1 vol. % of lithic fragments and reaching a maximum thickness of 5 cm. Towards >13 km to the NW of Masaya caldera, C2 grades into a ~1 cm thick black ash layer. C2 is a useful marker bed due to the fluidal morphology and high vesicularity of the glassy scoria.

At the most proximal exposures, C3 consists of several intercalated tuff and lapilli beds. Three main layers can be distinguished across the medial range: a fine yellowish indurated tuff with leaf molds at the base, a moderately well-sorted normal-graded layer of scoria lapilli and a relatively large fraction of lithic angular dense aphyric basaltic lava fragments (~5-15 vol. %, some hydrothermally altered) in a matrix of coarse ash (~30 vol. %), and a topmost thin hard tuff with desiccation cracks at the surface. All particles are coated with brownish fine ash. Plant remains from the basal tuff have been radiocarbon dated to 2,120 ± 120 years BP (Pérez and Freundt, 2006).

C7 is >40 cm thick yellowish tuff with abundant accretionary lapilli (diameters 2-10 mm) and scarce armored lapilli, is stratified by horizons enriched in lapilli or coarse-ash fragments, or accretionary lapilli. The quality of this texture varies between outcrops from apparently massive to well bedded; different degrees of induration locally emphasize the bedding.

C10 is the thickest and coarsest lapilli layer of the Managua facies, with a maximum observed thickness of 36 cm at 10 km to the NW of the caldera, decreasing to 3 cm near Ciudad Sandino (~25 km from the Masaya caldera). This well-sorted deposit of scoria lapilli is typically reversely graded at medial exposures but grading patterns are more variable at proximal outcrops, with two reversely graded horizons or symmetrical grading with largest grain size near the center.

3. Correlation between the facies

The different internal architectures of La Concepción and Managua facies do not allow to easily correlate individual layers, especially because there are no linking outcrops southwest and northeast the caldera. Yet both facies occur in the same stratigraphic position (Pérez and Freundt, 2006). Here we use chemical compositions to show that they are derived from the same magma batch. Based on that supposition, we then use petrographic and lithologic criteria to propose a layer-by-layer correlation.

3.1 Chemical compositions

A detailed stratigraphic sampling of several exposures at variable distances and directions from the Masaya caldera allowed us to compare the chemical compositions of bulk rock, matrix and inclusion glasses and mineral phases. Both, La Concepción and the Managua facies, are tholeiitic basalts and have completely overlapping bulk rock major and trace element compositions (Figs. 4, 9). These compositions are the least evolved of, and hence distinct from, the compositions of the other mafic tephras produced by the Masaya system (Fig. 4). They also differ in composition and by their young age from the Las Sierras Formation tephras.

The basaltic-andesitic compositions of the matrix glasses from both facies overlap completely in both major and trace elements (Fig. 9a, b); their displacement from whole-rock compositions largely reflects the abundance of plagioclase crystals in the latter. Moreover, the basaltic to basaltic andesitic glass inclusions, mostly hosted in plagioclase phenocrysts, show no compositional differences between the facies (Fig. 9c).

Likewise, the minerals in the scoriae of both facies are compositionally identical (Fig. 9d). The dominant mineral phase is calcic plagioclase ranging from An_{73} to An_{89}, and the microlites in the groundmass are at the calcic end of this range. The olivines of the LCF have Mg-numbers between 0.72-0.74, while those of the MF have a wider range of 0.70-0.82. Augites of Wo_{39-41} En_{45-48} Fs_{11-15} compositions with 0.47-0.57 wt% TiO_2 and 2.2 to 3.9 wt% Al_2O_3 are the same in both facies.

All these chemical criteria demonstrate that the two facies represent the deposit of one eruption of a single basaltic magma. Vertical changes show that this magma was somewhat heterogeneous in composition. Bulk-rock scoria compositions slightly increase in Al_2O_3 and decrease in TiO_2, Ba, FeO and alkalis upward through the deposit. An-contents of plagioclase phenocrysts increase upward and layers C1, C4 and C10 contain olivines with the widest range in Mg-numbers. The vertical compositional changes, however, are too subtle to be used for a detailed correlation of the two facies successions. Correlations must thus be based on lithologic characteristics such as scoria texture.

3.2 Proposed correlation

Two well-sorted layers, B5 of the LCF and C2 of the MF, are prominent in their respective facies because they consist entirely of highly vesicular, fluidally-textured elongate achneliths (see Fig. 7). Masaya volcano has repeatedly produced such scoria particles in eruptions ranging from the ~6 ka San Antonio Tephra (Pérez and Freundt, 2006) to the recent products of active Santiago crater. In the MTL, however, their dominant occurrence is limited to two layers. We therefore use the correlation B5=C2 as a starting point to merge the layers of the two facies into 10 correlated depositional units (I-X) based on similar lithologic and petrographic properties. The combined stratigraphy agrees with the overall upward increase in less vesicular scoria particles and hydrothermally altered lithics observed in both facies. Each new subunit has been checked for consistency of the resulting areal thickness and grain-size distributions. The most plausible correlation scheme between La Concepción and Managua facies is illustrated in figure 10. The major well-sorted lapilli fallout layers of both facies are correlated resulting in subunits II (B5, C2), IV (B9, C4), VI (B11, C6), VIII (B14, C8) and X (B16, C10). The areal distributions of these fallouts and their volcanological significance are discussed below. First, we summarize the implications for the tuff deposits.

Subunit I consists of layers B0 to B4 which thin to the NW and merge into layer C1, which contains a horizon rich in plant material resembling B2. The opening phase of the MTL eruption represented by subunit I began with minor phreatomagmatic ash fallouts (B0) followed by a more intense eruption emplacing the first lapilli fallout B1, which is interrupted by a weak ash surge (B2) before a weaker column is re-established (fallout B3) that finally collapsed when a wet surge (B4) was erupted. The distal fallout of B1 and B3 is combined in layer C1.

Subunit III includes the two surge layers B6 and B8, which are separated by the lapilli fallout B7. This tri-partite structure is preserved in a condensed fashion in the distal layer C3 in the NW.

Subunit V combines the tuffs B10 and C5 and represents the deposit of a major, energetic wet surge event.

Subunit VII is a surge deposit (B12) capped by a tuff rich in accretionary lapilli (B13) that forms a single thick accretionary-lapilli-rich tuff (C7) distally in the NW, probably the deposit of wind-driven ash clouds of the surges.

Subunit IX (B15, C9) has characteristics of an ash-rich surge that –in contrast to the earlier surges– expanded more strongly to the NW and was weaker to the S. The deposit is everywhere capped by an indurated thin fine-ash layer, the final wet fallout from the surge cloud.

Desiccation cracks at the tops of subunits III, V and IX indicate significant breaks in the eruptive activity and dry warm weather conditions as also supported by the absence of erosion. The areal thickness distribution of the tuff subunits is controlled by topography, as shown by the isopach maps of subunits V, VII and IX (Fig. 11). However, the major pyroclastic surges were not restricted to low flat areas but surmounted the Las Sierras hills west of the Masaya caldera to produce significant deposits on their lee flanks.

4. The major fallout deposits

Preliminary estimates of eruption parameters for the entire deposit, based on separate treatment of the LCF and MF fallout data, have been given by Pérez and Freundt (2006) and Kutterolf et al. (2007). Here we re-interpret the data using isopach and isopleth maps of the major fallout subunits defined by the proposed correlation between the facies. These isopach and isopleth maps remain poorly constrained southwest and northeast of the caldera where MTL outcrops are lacking. Thickness data for subunit VII to X to the south are scarce due to post-emplacement erosion of the top of the MTL. Vent positions cannot be determined precisely because proximal outcrops are restricted to the area close to the southern caldera rim. Nevertheless, all isopach maps indicate a vent inside the Masaya caldera, possibly beneath the modern Masaya intra-caldera cone.

4.1 Dispersal characteristics

The isopach maps for the correlated fallout subunits I, III, IV, VI, and X all show a dispersion towards the NW, in direction to Managua city (Fig. 11). In detail, however, there are differences in the isopach elongation and axis orientation between subunits, indicating changing wind conditions. For example, the concentric circular pattern of subunit II isopachs indicates calm conditions whereas a strong wind blowing toward the NW generated the elongated isopachs of subunit IV.

All major fallout subunits show a gradual decay in thickness with distance, typical for Plinian-type deposits (Fig. 12). Minor variations in thickness decrease between the subunits reflect variations in eruption intensity. Moreover, values of thickness half-distance (b_t) and clast half-distance (b_c) for these deposits of 2.6-3.9 km and 6-18 km, respectively, are in the ranges typical for Plinian eruptions (Pyle, 1989).

The frequent interruption of the Plinian-type eruptions by phreatomagmatic, typically surge-producing events, suggests that external water affected all eruptive pulses but to variable extent. Subunits II and IV are relatively lithic-poor, well-sorted, and contain a large fraction of highly vesicular scoria lapilli. We interpret these as mainly magmatic Plinian eruptions (while noting that the presence of partially quenched lapilli indicates access of some water to the conduit). On the other hand, subunits III, VI and X are moderately sorted (σ>1.5), more lithic-rich and most of the scoriae are poorly vesicular; moreover, scoria lapilli in subunit III are ash-coated and proximally intercalated with tuff layers. We interpret these eruptive events as Phreatoplinian since they were clearly more strongly affected by magma-water interaction. Fallout subunit VIII shows locally variable faint parallel or cross-bedding; this may be due to surge-blast expansion contemporaneous with fallout emplacement but may also have been caused by strong near-surface wind.

4.2 Eruption column heights and wind speed

We use downwind and crosswind ranges obtained from isopleth maps of maximum juvenile (MP) and lithic fragments (ML) of the fallout subunits II, III, IV, VI, VIII and X for comparison with eruption-column modeling results of Carey and Sparks (1986) to estimate eruption column heights and wind speeds (Fig. 13). The resulting overall range in column heights is 15 to 32 km. The best-constrained values suggest 22-24 km for subunit II, 22-28 km for subunit III, 21-23 km for subunits IV and VI, and 26-32 km for subunit X. Magma mass discharge rates can be estimated from eruption column heights by comparison with the model results of Woods (1988). Resulting discharge rates for the fallout subunits lie between 10^7 to 10^8 kg/s (Fig. 14), with subunit X having the highest discharge close to 10^8 kg/s.

Estimated wind speeds are <2 m/s for subunit II in agreement with its concentric circular isopach and isopleth patterns, around 10 m/s for subunits III, IV and VI, and ~20 m/s for the topmost subunit X. These differences reflect changes in wind strength both with time and with height in the atmosphere. The data in figure 13 suggest that the coarser material emplaced within 5-10 km from vent never reached the stratosphere and that its dispersal was controlled by tropospheric winds. Different tropospheric and stratospheric wind directions and strengths caused bends in dispersal axes of some fallout deposits. The isopach pattern of subunit III extends proximally westward before turning toward NW, and subunit VI proximally extends to the S while the main fan is directed to the NW. On the other hand, the distal fallouts from wind-driven surge clouds all extend to the NW; this may suggest that near-surface wind directions were more constant than those in the higher troposphere. Present-day winds at the surface and in the stratosphere (cf. Kutterolf et al., 2007) blow westward throughout the year but change in the upper troposphere from northeastern directions during the dry season to southwestern directions during the rainy season. If similar conditions prevailed 2 ka ago, subunits V and VI, with proximally southerly dispersal, would have been erupted during the rainy season. On the other hand, desiccation cracks at the surface of subunits III, V and IX suggest dry and hot weather. The different transport and wind conditions, indications of breaks in volcanic activity, as well as the changes in eruption style support that the MTL eruption consisted of numerous separate episodes that occurred over an extended period of time, possibly several months. Individual fallout episodes may have lasted 1-3 hours judging from mass discharge rates and erupted masses discussed in the next section.

4.3 Volume

The subunit tephra volumes range from 0.02 to 0.22 km^3 (Table 3) and are equivalent to erupted magma masses between 10^{10} and 10^{11} kg. The fallout subunits II, III and X represent the eruptive episodes with the largest magnitudes. The added-up total tephra volume of the Masaya Triple Layer is 0.86 km^3, a minimum estimate based on land outcrops.

Two ash layers found in sediment cores drilled at the continental slope ~170 km away from the Masaya caldera have been correlated with the Masaya Triple Layer based on their identical major and trace element chemical compositions, as well as other criteria, e.g. stratigraphic position of other dated and correlated ash layers in the core, mineral assemblages and texture of the glass shards (Kutterolf et al., 2008a). The ash layer in core M54/2 is 6 cm thick, the one in core SO173/3-18 4 cm (Fig. 15). These data imply a much flatter thickness decay distally than on land (see inset in Fig. 12) and hence yield a significantly increased tephra volume of the MTL of 3.4 km^3 (~1.8 km^3 DRE, after Kutterolf et al., 2008b). The additional distal volume must be attributed to the major fallout events because the intercalated tuffs from phreatomagmatic pulses do not reach that far.

The land isopachs show a major dispersion axis towards the northwest, whereas the distal isopachs suggest transport to the west, reflecting wind directions changing with height. This decoupling in transport direction has been reported for several eruptions around the world (e.g. Sarna-Wojcicki et al., 1981; van den Bogaard and Schmincke, 1984; Adams et al., 2001). A similar pattern to that of the MTL is exhibited by the 25 ka Upper Apoyo Tephra (Kutterolf et al., 2007, 2008a), coinciding with stratospheric winds to the west above 27 km height and lower tropospheric winds to the west-northwest (see Kutterolf et al., 2007).

5. The Masaya Triple Layer eruption

Two facies of volcanic deposits that occur in different areas to the N and S of Masaya caldera at the same stratigraphic position have identical magmatic compositions and are thus the deposit of a single eruption although they differ in internal architectures. La Concepción facies of the Masaya Triple Layer is the more proximal facies of the eruption south of the caldera, deposited in an area where fallout was still controlled by tropospheric rather than stratospheric winds and where a rougher topography controlled the flow paths of the surges. The Managua facies of the MTL, on the other hand, includes the medial and distal deposits in the direction of fallout dispersion by stratospheric wind and of fine-ash fallout from surge-related ash-clouds driven by near-surface wind. Using the proposed correlation between the two facies (Fig. 10), we summarize the evolution of the MTL eruption in figure 16. The MTL eruption consisted of many episodes separated by time breaks sufficiently long for atmospheric wind conditions to change and for desiccation cracks to form on the surface of ash emplaced wet. The eruption style varied between phreatomagmatic explosions and sustained Plinian and Phreatoplinian eruption columns that reached high into the stratosphere.

The eruption started with phreatomagmatic precursor activity, producing ash fall (B0, **subunit I**) limited to proximal areas south of the caldera. The first main eruptive episode began with minor phreatomagmatic fallout (B1) and minor surges that ripped off vegetation, then became more magmatic with fallout B3 but terminated with another phreatomagmatic eruption of ash fallout (B4). Opening and widening of the vent probably contributed to the relatively high lithic contents of these deposits. The next episode (**subunit II**) was the first major magmatic Plinian eruption that evacuated 0.038 km^3 of fresh non-degassed magma and formed an eruption column of 22-24 km height lasting for ~1 h (derived by dividing DRE mass by mass flux). Vertical grain-size variations suggest the eruption to have fluctuated in intensity while fallout dispersal was concentric under calm wind conditions. The characteristic fluidal shapes of the lapilli (achneliths) indicate eruption of a hot low-viscosity magma that remained unaffected by contact with external water.

The next episode (**subunit III**) was mostly phreatomagmatic, forming surges that destroyed and carried along the vegetation. Intermittent ~22-28 km high eruption columns were unstable and collapsed to form minor surges. A break in activity (desiccation cracks on tuff surface) preceded the second major Plinian eruption (**subunit IV**), during which water access to the conduit was largely inhibited and which took a couple of hours to eject 0.025 km^3 of magma in an eruption column rising to 21-23 km. When water regained access to the conduit, the following phreatomagmatic episode (**subunit V**) formed surges that flowed mainly towards the south, whereas their ash-clouds were driven towards the NW by near-surface wind. Desiccation cracks at the top of the tuff indicate another major break after this episode. The MTL eruption started again with a Phreatoplinian eruption column (**subunit VI**) of similar dimensions than during the subunit-IV episode but more strongly affected by external water as evidenced by the higher fraction of hydrothermally altered lithics and poorly vesicular scoriae. Increasing flux of water into the conduit then resulted in the largest phreatomagmatic episode of the entire eruption (**subunit VII**) that produced thick surge deposits to the S and associated ash-cloud deposits rich in accretionary lapilli to the NW. A low-intensity phreatomagmatic episode (**subunit VIII**) followed and formed a fine-grained, relatively well-sorted deposit with faint cross bedding, suggesting fallout with a minor lateral transport component possibly from a low drifting ash cloud. The next episode had regained higher intensity and mainly generated phreatomagmatic surges of widespread distribution (**subunit IX**). Another significant break in activity allowed for desiccation cracks to form on the surface of this deposit. The terminal episode of the MTL eruption (**subunit X**) was the most vigorous event with a 26-32 km high Phreatoplinian eruption column fed by a relative high magma discharge rate. The fallout dispersal of the ~0.1 km^3 of magma was mainly controlled by strong stratospheric winds. The nature of the juvenile fragments and the high fraction of lithic clasts, some hydrothermally altered, suggest intense magma-water interaction.

6. Conclusions

The Masaya Triple Layer provides an example of the complex evolution of a basaltic Plinian eruption. The repeated alternation between clearly phreatomagmatic tuffs and fallout deposits ranging from “magmatic” to “phreatomagmatic” characteristics suggests that external water to some extent controlled the eruptive style of all eruption events such that even the explosivity of the apparently magmatic events may have been increased by water vaporization. Peaks in water access generating phreatomagmatic explosions were followed by breaks in eruptive activity (desiccation cracks at the top of tuff layers), perhaps due to exhaustion of the water reservoir and the necessity for the magma system to build up pressure for the next eruption. Therefore, the MTL Plinian eruption was not only unsteady but multi-episodic, lasting for weeks or months with intervening extended periods of inactivity. This is a critical issue for hazard assessments, because major break during an eruption may be mistaken for the end of the eruption while, as shown for the MTL eruption, the most powerful event may still be coming.

Acknowledgments

This publication is contribution No. 140 of the Sonderforschungsbereich (SFB) 574 "Volatiles and Fluids in Subduction Zones" at Kiel University. This work was part of W. Pérez PhD thesis, which was partly supported by the German Academic Exchange Service (DAAD). We thank the Instituto Nicaragüense de Estudios Territoriales (INETER) for logistic support in the field. S. da Silva and J. Fierstein provided constructive revisions that improved this paper.

References

Adams, N.K., de Silva, S.L., Self, S., Salas, G., Schubring, S., Permenter, J.L., Arbesman, K., 2001. The physical Volcanology of the 1600 eruption of Huaynaputina, southern Peru. Bull. Volcanol. 62, 493-518.

Barckhausen, U., Ranero, C.R., von Huene, R., Cande, S.C. and Roeser, H.A., 2001. Revised tectonic boundaries in the Cocos plate off Costa Rica: Implications for the segmentation of the convergent margin and for plate tectonic models. J. Geophys. Res. 106, 19207-19220.

Bice, D.C., 1985. Quaternary volcanic stratigraphy of Managua, Nicaragua: Correlation and source assignment for multiple overlapping plinian deposits. Geol. Soc. Amer. Bull. 96, 553-566.

Carey, S., Sparks, R.S.J., 1986. Quantitative models of fallout and dispersal of tephra from volcanic eruption columns. Bull. Volcanol. 48, 109-125.

Carey, R., Houghton, B.F., Sable, J.E., Wilson, C.J.N., 2007. Contrasting grain size and componentry in complex proximal deposits of the 1886 Tarawera basaltic Plinian eruption. Bull. Volcanol. 69, 903-926.

Coltelli, M., Del Carlo, P., Vezzoli, L., 1998. Discovery of a Plinian basaltic eruption of Roman age at Etna volcano, Italy. Geology 26, 1095-1098.

Costantini, L., Bonadonna, C., Houghton, B.F., Wehrmann, H., 2008. New physical characterization of the Fontana Lapilli basaltic Plinian eruption, Nicaragua. Bull. Volcanol (in press).

DeMets, C., 2001. A new estimate for present-day Cocos-Caribbean plate motion: Implications for slip along the Central American volcanic arc. Geophys. Res. Lett. 28, 4043-4046.

Duffell, H.J., McGonigle, A.J.S., Burton, M.R., Oppenheimer, C., Pyle, D.M., and Galle, B., 2003. Changes in gas composition prior to a minor explosive eruption at Masaya volcano, Nicaragua. J. Volcanol. Geotherm. Res. 126, 327-339. doi:10.1016/S0377–0273(03)00156–2.

Dzurisin, D., Lockwood, J.P., Casadevall, T.J. and Meyer, R., 1995. The Uwekahuna Ash Member of the Puna Basalt: product of a violent phreatomagmatic eruptions at Kilauea volcano, Hawaii, between 2800 and 2100 14C years ago. J. Volcanol. Geotherm. Res. 66, 163-184.

Fierstein, J., Nathenson, M., 1992. Another look at the calculation of fallout tephra volumes. Bull. Volcanol. 54, 156-167.

Girard, G., van Wyk de Vries, B., 2005. The Managua Graben and Las Sierras-Masaya volcanic complex (Nicaragua); pull-apart localization by an intrusive complex: results from analogue modeling. J. Volcanol. Geotherm. Res. 144, 37-57.

Houghton, B.F., Wilson, C.J.N., 1989. A vesicularity index for pyroclastic deposits. Bull. Volcanol. 51, 451-462.

Houghton, B.F., Wilson, C.J.N. and Pyle, D.M., 2000. Pyroclastic fall deposits. In: H. Sigurdsson, B.F. Houghton, S. McNutt, H. Rymer, J. Stix (Editors), Encyclopedia of volcanoes, Academic Press, San Diego, pp 555–570.

Horrocks, L., Burton, M., Francis, P., Oppenheimer, C., 1999. Stable gas plume composition measured by OP-FTIR spectroscopy at Masaya volcano, Nicaragua, 1998-1999. Geophys. Res. Lett. 26, 3497-3500.

Kutterolf, S., Freundt, A., Peréz, W., Mörz, T., Schacht, U., Wehrmann, H., Schmincke, H.-U., 2008a. The Pacific offshore record of Plinian arc volcanism in Central America: 1. Along-arc correlations. Geochemistry, Geophysics, Geosystems 9. doi:10.1029/2007GC001631

Kutterolf, S., Freundt, A., Peréz, W., 2008b. The Pacific offshore record of Plinian arc volcanism in Central America: 2. Tephra volumes and erupted masses. Geochemistry, Geophysics, Geosystems 9. doi:10.1029/2007GC001791.

Kutterolf, S., Freundt, A., Pérez, W., Wehrmann, H. and Schmincke, H.-U., 2007. Late Pleistocene to Holocene temporal succession and magnitudes of highly-explosive volcanic eruptions in west-central Nicaragua. J. Volcanol. Geotherm. Res. 163, 55-82.

Lewicki, J.L., Connor, C., St-Amand, K., Stix, J., Spinner W., 2003. Self-potential, soil CO2 flux, and temperature on Masaya volcano, Nicaragua. Geophys. Res. Lett. 30, 1817. doi:10.1029/2003GL017731

Mastin, L.G., 1997. Evidence for water influx from a caldera lake during the explosive hydromagmatic eruption of 1790, Kilauea volcano, Hawaii. J. Geophys. Res. 102, 20093-20109.

McBirney, A.R., 1956. The Nicaraguan volcano Masaya and its caldera. Amer. Geophys. Union Transactions 37, 83-96.

McPhie, J., Walker, G.P.L., Christiansen, R.L., 1990. Phreatomagmatic and phreatic fall and surge deposits from explosions at Kilauea volcano, Hawaii, 1790 A.D.: Keanakakoi Ash Member. Bull. Volcanol. 52, 334-354.

Métaxian, J.-Ph., Lesage, Ph., Dorel, J., 1997. The permanent tremor of Masaya volcano, Nicaragua: Wave field analysis and source location. J. Geophys. Res. 102, 22,529-22,545.

Pérez, W., Freundt, A., 2006. The youngest highly explosive basaltic eruptions from Masaya Caldera (Nicaragua). In: W.I. Rose, G.J.S. Bluth, M.J. Carr, J.W. Ewert, L.C. Patino, J.W. Vallance (Editors), Volcanic hazards in Central America. Geol. Soc. Am. Spec. Pap. 412, pp 189-207.

Pyle, D.M., 1989. The thickness, volume and grain-size of tephra fall deposits. Bull. Volcanol. 51, 1-15.

Rymer, H., van Wyk de Vries, B., Stix, J., Williams-Jones, G., 1998. Pit crater structure and processes governing persistent activity at Masaya Volcano, Nicaragua. Bull. Volcanol. 59, 345-355.

Sable, J.E., Houghton, B.F., Wilson, C.J.N., Carey, R.J., 2006. Complex proximal sedimentation from Plinian plumes: the example of Tarawera 1886. Bull. Volcanol. 69, 89-103.

Sarna-Wojcicki, A.M., Shipley, S., Waitt, J.R., Dzurisin, D., Wood, S.H., 1981. Areal distribution, thickness, mass, volume and grain-size of air-fall ash from the six major eruptions of 1980. U. S. Geol. Surv. Prof. Pap. 1250, 577- 600.

Sparks, R.S.J., Bursik, M.I., Ablay, G.J., Thomas, R.M.E., Carey, S.N., 1992. Sedimentation of tephra by volcanic plumes. Part 2: controls on thickness and grain-size variations of tephra fall deposits. Bull. Volcanol. 54, 685-695.

Stoiber, R.E., Williams, S.N., 1986. Sulfur and halogen gases at Masaya caldera complex, Nicaragua: Total flux and variations with time. J. Geophys. Res. 91, 12,215-12,231.

van den Bogaard, P., Schmincke, H.-U., 1984. The eruptive center of the Late Quaternary Laacher See Tephra. Geol. Rdsch. 73, 933-980.

van Wyk de Vries, B., 1993. Tectonics and magma evolution of Nicaraguan volcanic systems. Ph.D. Thesis. Open Univ., UK.

Walker, G.P.L., Self, S., Wilson, L., 1984. Tarawera 1886, New Zealand - A basaltic Plinian fissure eruption. J. Volcanol. Geotherm. Res. 21, 61-78.

Walker, J.A., Williams, S.N., Kalamarides, R.I., Feigenson, M.D., 1993. Shallow open-system evolution of basaltic magma beneath a subduction zone volcano: the Masaya Caldera Complex, Nicaragua. J. Volcanol. Geotherm. Res. 56, 379-400.

Wehrmann, H., Bonadonna, C.B., Freundt, A., Houghton, B.F., Kutterolf, S., 2006. A basaltic-andesitic plinian eruption revisited: case study of Fontana Tephra, Nicaragua. In: W.I. Rose, G.J.S. Bluth, M.J. Carr, J.W. Ewert, L.C. Patino, J.W. Vallance (Editors), Volcanic hazards in Central America. Geol. Soc. Am. Spec. Pap. 412, pp. 209-223.

Wehrmann, H., 2005. Volatile degassing and Plinian eruption dynamics of the mafic Fontana Tephra, Nicaragua. Ph.D. Thesis. Kiel Univ., Germany.

Williams, S.N., 1983. Plinian airfall deposits of basaltic composition. Geology 11, 211-214.

Wilson, L., Walker, G.P.L., 1987. Explosive volcanic eruptions: VI. Ejecta dispersal in plinian eruptions: the control of eruption conditions and atmospheric properties. Geophys. J. R. Astron. Soc. 89, 657–679.

Woods, A.W., 1988. The fluid dynamics and thermodynamics of eruption columns. Bull. Volcanol. 50, 169-193.

Figure Captions

Figure 1: Digital elevation model of Nicaragua showing the two large lakes, the position of the volcanic front and the location of the Masaya Caldera Complex. The black stippled line marks the boundary of the Nicaraguan depression after van Wyk de Vries (1993).

Figure 2: Facies distribution of the Masaya Triple Layer, with La Concepción facies (LCF) to the south of the caldera and the Managua facies (MF) to the northwest. The open circles and squares represent the studied localities and the red lines connect the proximal profiles shown in figures 4 and 7. Note the lack of MTL outcrops to the west (direction to El Crucero) and northeast (towards Tipitapa).

Figure 3: End-member types of juvenile fragments of the Masaya Triple Layer in thin section: [**a**] highly vesicular sideromelane (~80 vol. % porosity), [**b**] moderately vesicular tachylite with ~40 vol. % round vesicles and [**c**] incipiently vesicular tachylite, where the vesicularity consists of irregular-shaped voids (~16 vol. %).

Figure 4: Diagram SiO_2 vs. MgO comparing the composition of the two facies of the Masaya Triple Layer (La Concepción facies -LCF- and Managua facies -MF-) with the composition fields of other major tephra units from Masaya caldera (SAT=San Antonio Tephra, MT=Masaya Tuff, TIL=Ticuantepe Lapilli) and the older Las Sierras volcanic system (FT=Fontana Tephra, LSF=Las Sierras Formation; data from Wehrmann (2005) and own unpublished data).

Figure 5: Proximal stratigraphy of La Concepción facies, south of the caldera. The profile line is shown in Fig. 2. Gray shading correlates lapilli beds between outcrops. Note the different degrees of erosion at the top of the outcrops, with the Masaya Tuff lying unconformably above.

Figure 6: Photographs of the juvenile particles of layer B5. [**a**] Selected particles with fluidal shapes and glassy surfaces. [**b**] Whole deposit as it looks in the outcrops. [**c**] Highly vesicular brown sideromelane glass in thin section.

Figure 7: Photographs of the tuff sequence B6-B10 with intercalated well-sorted fall deposits. [**a**] At an outcrop 3 km S from the caldera rim where the layers are several cm thick. [**b**] The three tuffs at 7.5 km S of the caldera rim.

Figure 8: Stratigraphy of the Managua facies at the most proximal exposures NW of the caldera. The profile line and location of the outcrops are shown in Fig. 2. Correlations between outcrops are indicated by gray shading.

Figure 9: Variation diagrams showing the complete overlap in: [**a**] major element (FeO vs. MgO) and [**b**] trace-element (Ba vs. Zr) compositions of matrix glass, [**c**] Al_2O_3 vs. CaO concentrations of melt inclusion glasses, and [**d**] K_2O vs. CaO concentrations in plagioclase phenocrysts from the Managua facies (MF) and La Concepción facies (LCF).

Figure 10: Proposed correlation between La Concepción and the Managua facies based on the marker beds B5 and C2 (subunit II, correlation in red). As indicated, the left profile -MF- is towards the NW of the caldera and the right profile -LCF- is to the S of Masaya caldera.

Figure 11: Isopach maps for the main fallout subunits I, II, III, IV, VI, X and the surge-tuff subunits V, VII and IX of the Masaya Triple Layer. Isopach contours are in cm and the dashed lines are estimated in areas with no data. The cities of Managua and Masaya are shown in gray.

Figure 12: Diagram of isopach thickness vs. square root of isopach area for the MTL fallout subunits. The fields of Plinian, Subplinian and Phreatoplinian eruptions are from Houghton et al. (2000). The inset at the top right corner shows the same diagram on a bigger scale for the entire MTL including the thickness data from the distal marine tephra layers.

Figure 13: Crosswind range versus maximum downwind range of the MP and ML isopleths for subunits II, III, IV, VI and X of the MTL. The model curves are from Carey and Sparks (1986). Most of the MTL data locate between 20 and 28 km column height and indicate different winds speeds for the subunits.

Figure 14: Eruption column height versus log of the mass eruption rate with the lines for different eruption temperatures of Woods (1988). The colored oval areas locate column heights for the fallout subunits II, III, IV, VI and X on the 1200 K line (eruption temperature for basaltic magmas). The eruption temperature of the poorly phyric basaltic MTL magma was probably 200 degrees higher such that mass eruption rates estimated from this figure are maximum estimates.

Figure 15: Isopachs in centimeters (dotted line) for the Masaya Triple Layer total thickness. The cross-circle symbols give the location of sediment gravity cores drilled offshore Nicaragua; labels indicate the core number and the thickness of the ash layer.

Figure 16**.** Schematic model of the Masaya Triple Layer eruption as discussed in the text, showing the main Plinian and Phreatoplinian eruptions interrupted by surge-forming phreatomagmatic activity. Blue lenses represent ground water accessing the conduit.

Fig 1


87°
86°
85°
84°
14°
13°
12°
11°
N
S
W
E
0
100 km
HONDURAS
NICARAGUA
Interior Highlands
Lake Managua
Lake Nicaragua
Nicaraguan Depression
Masaya Caldera Complex
Pacific Ocean
COSTA RICA

688 Fig 2

689

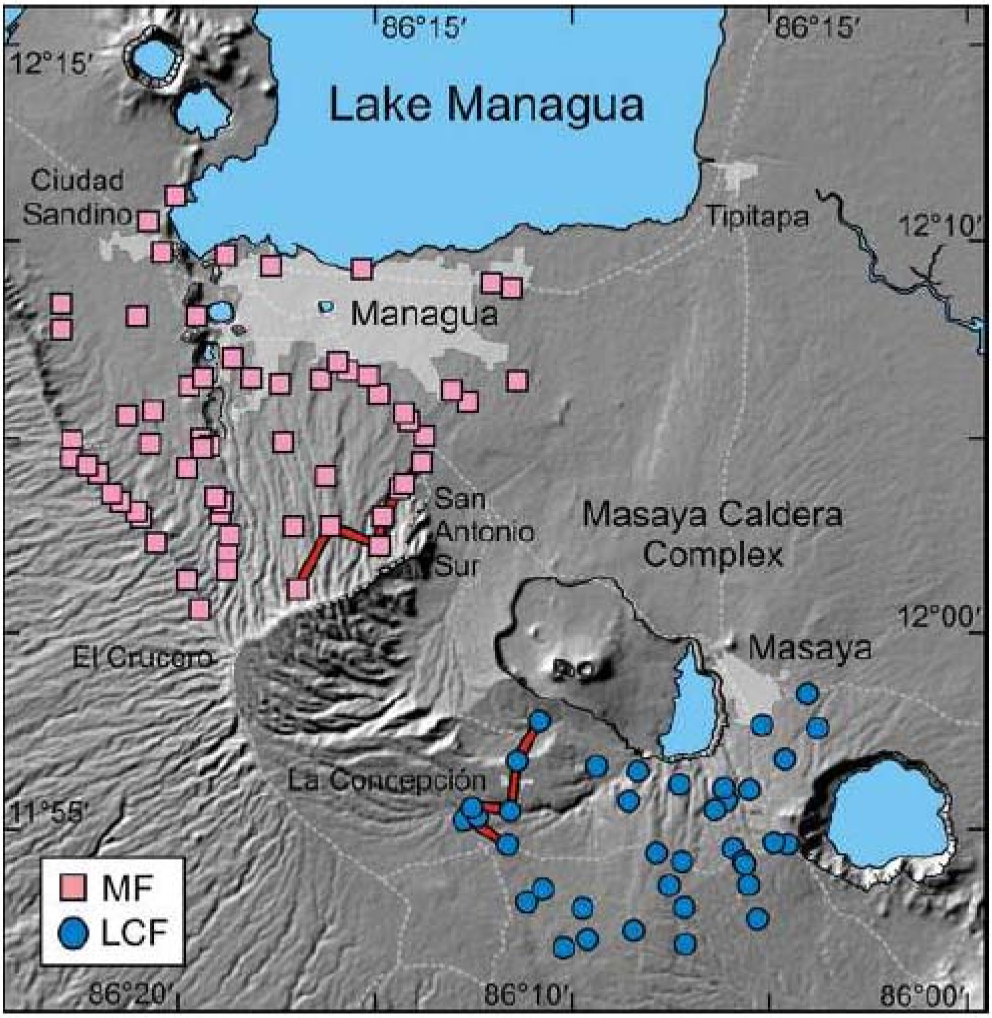

690

691 Fig 3

692

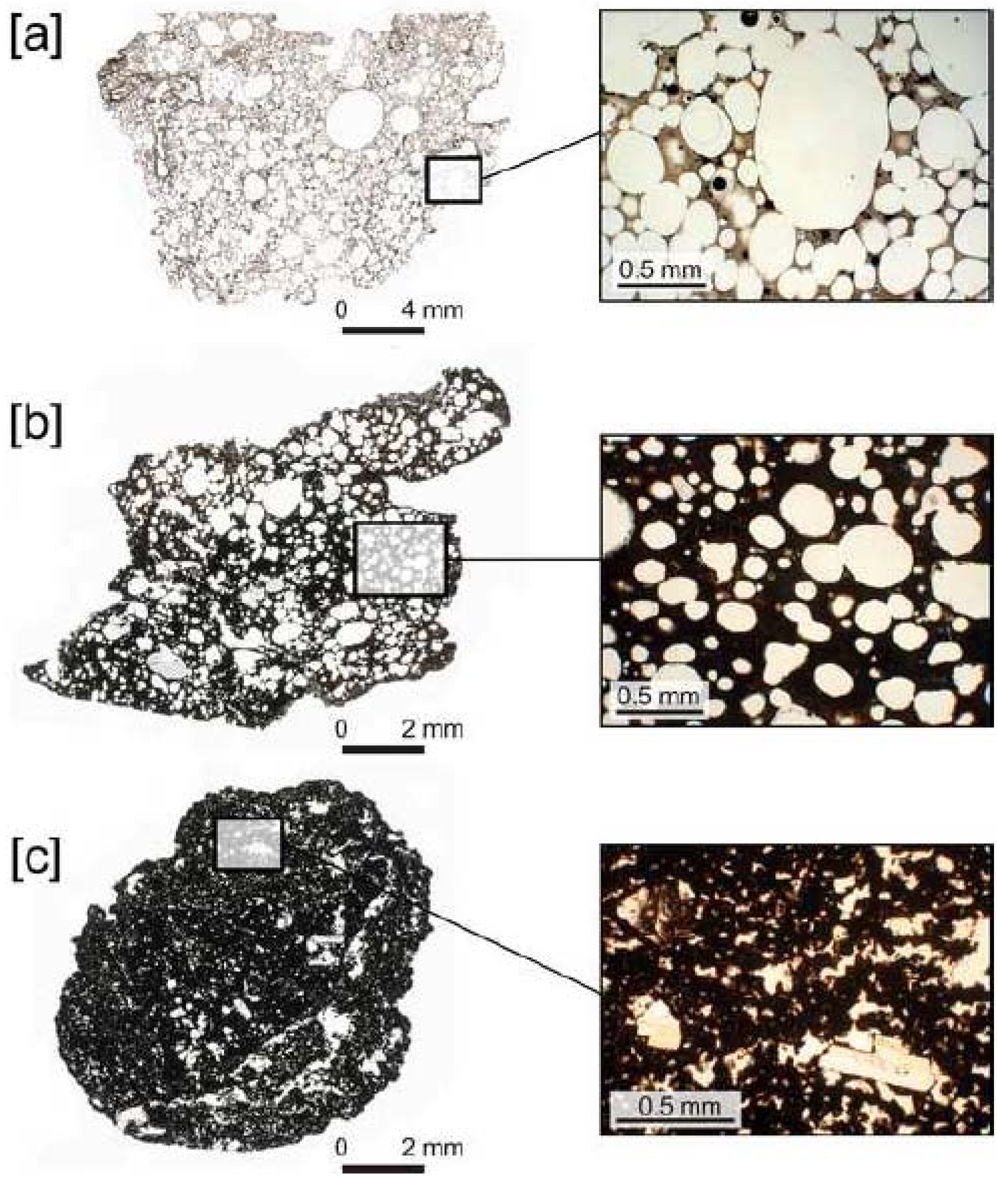

693

694 Fig 4

695

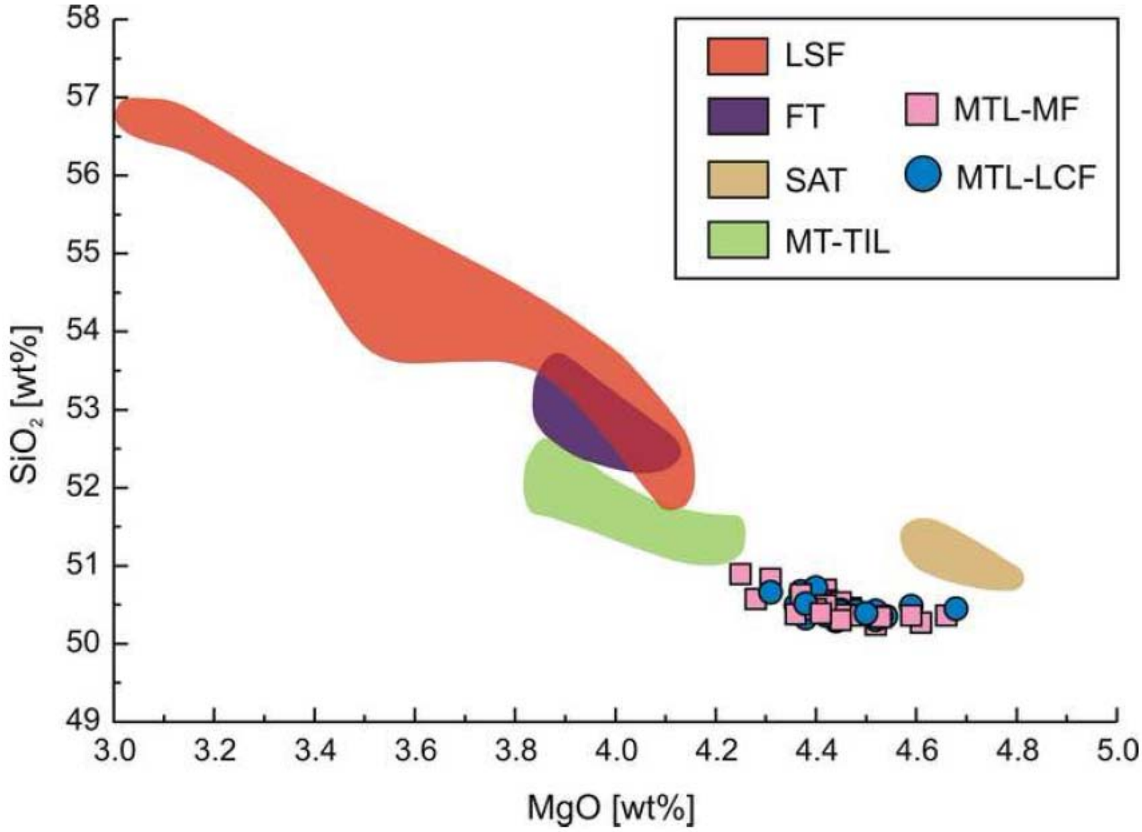

696

Fig 5

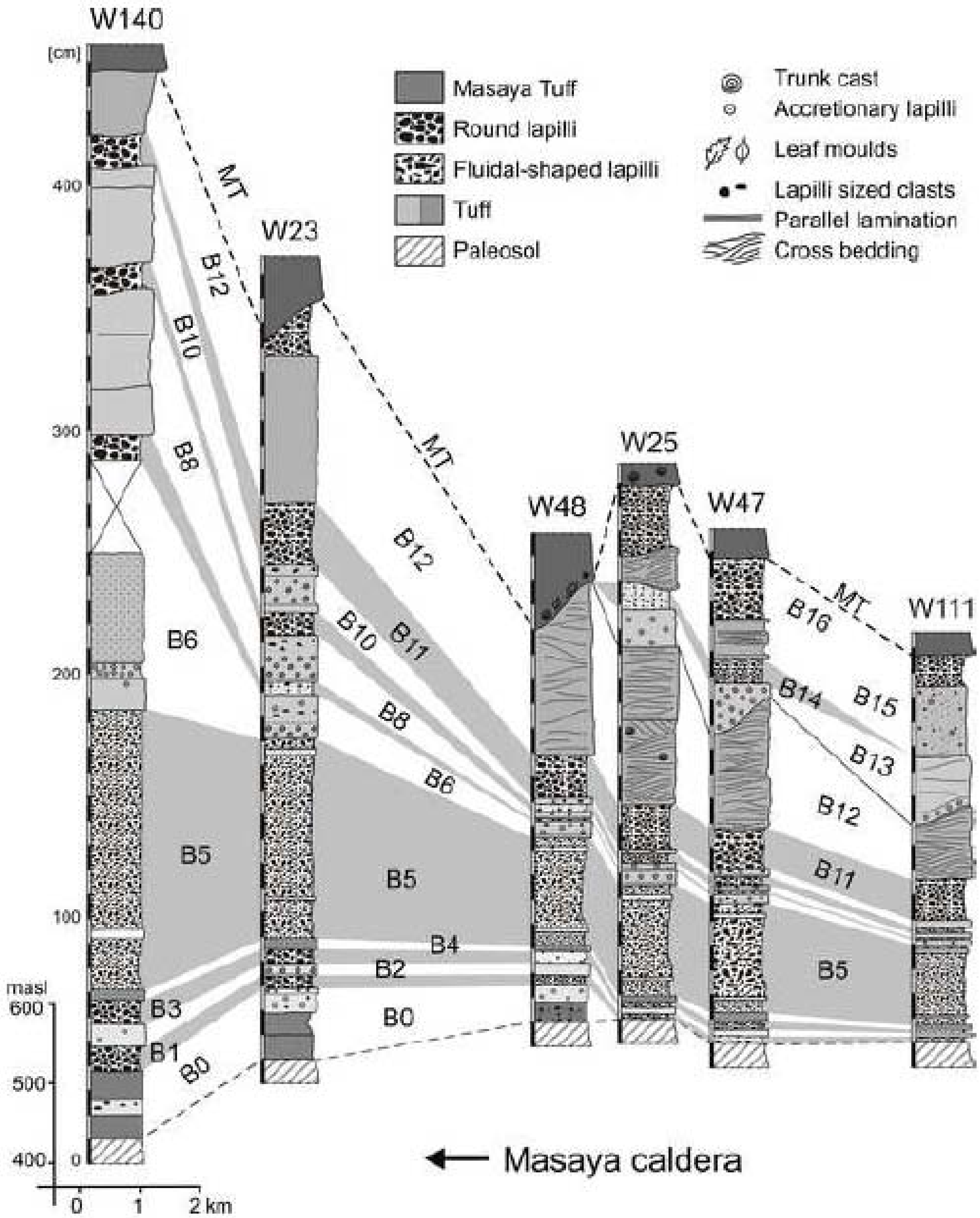
W140
[cm]
400
300
200
100
0
masl
600
500
400
0
1
2 km
W23
W48
W25
W47
W111
Masaya Tuff
Round lapilli
Fluidal-shaped lapilli
Tuff
Paleosol
Trunk cast
Accretionary lapilli
Leaf moulds
Lapilli sized clasts
Parallel lamination
Cross bedding
MT
B12
B10
B8
B6
B5
B4
B3
B2
B1
B0
B11
B16
B15
B14
B13
Masaya caldera

700 Fig 6

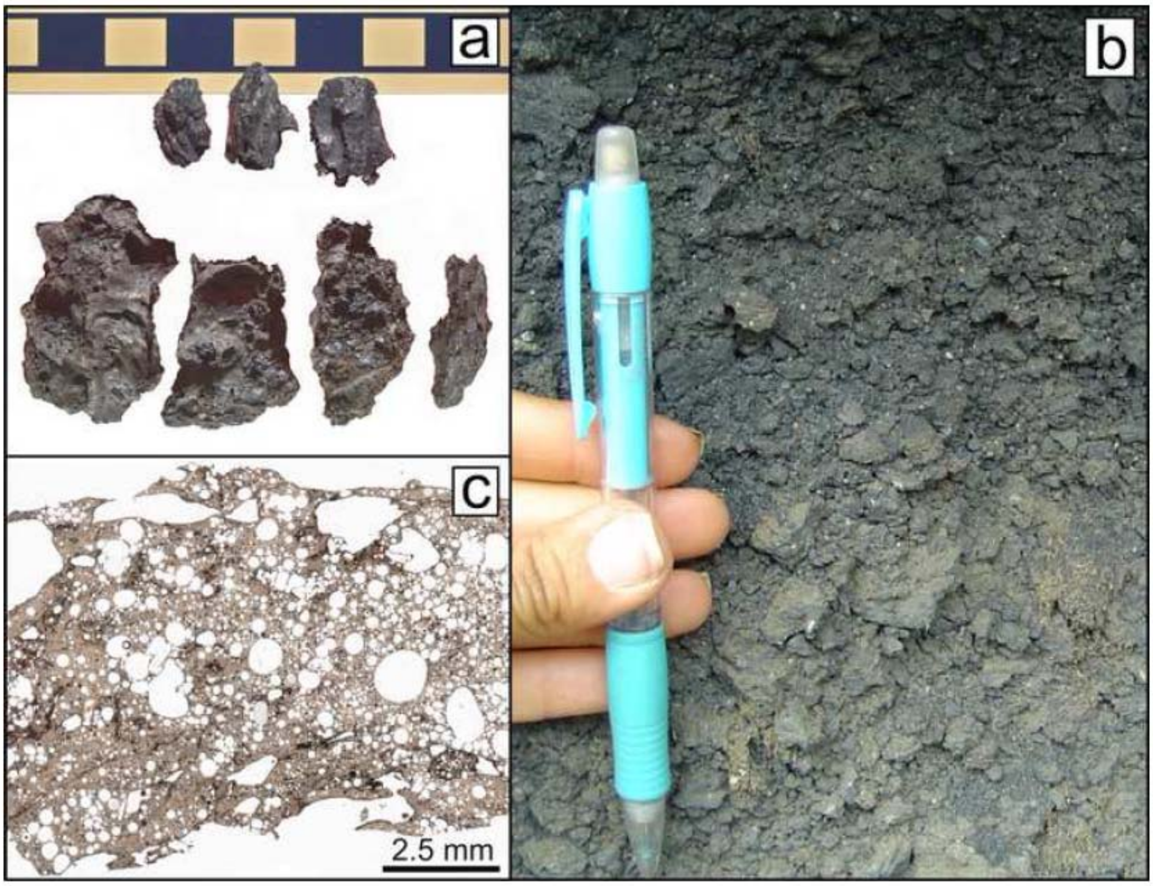

703 Fig 7
704

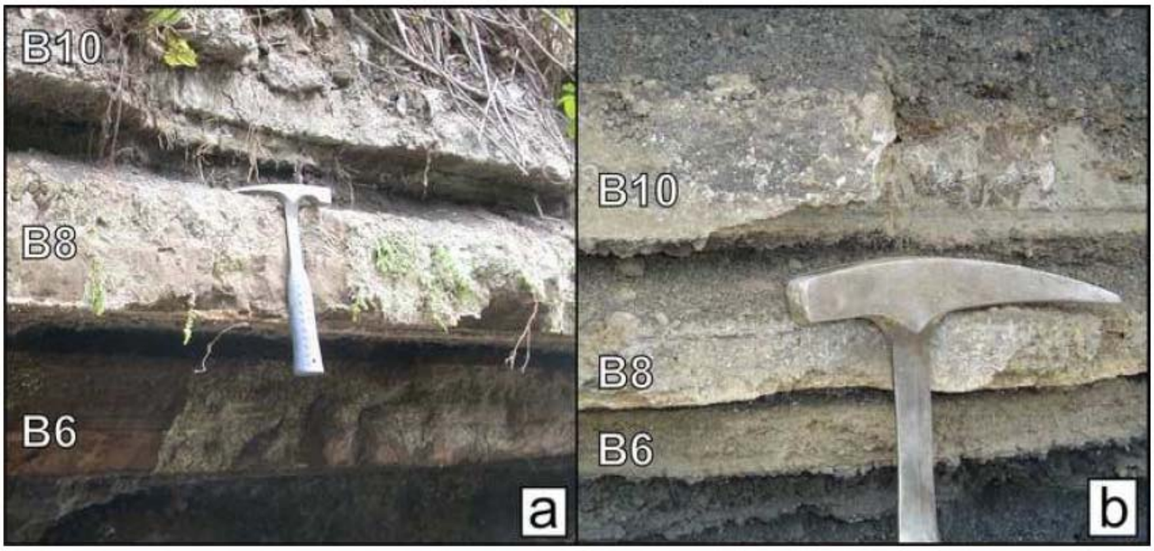

705

Fig 8

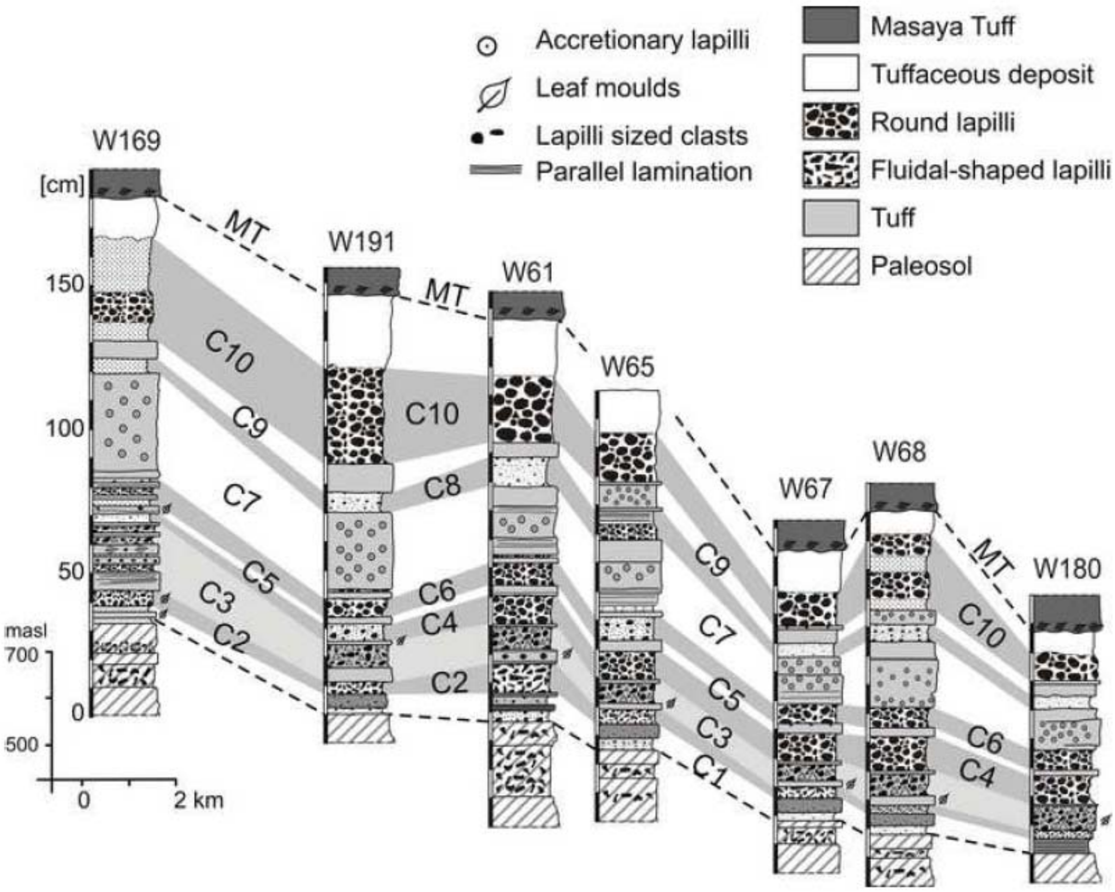

Accretionary lapilli
Leaf moulds
Lapilli sized clasts
Parallel lamination
Masaya Tuff
Tuffaceous deposit
Round lapilli
Fluidal-shaped lapilli
Tuff
Paleosol
W169
W191
W61
W65
W67
W68
W180
[cm]
150
100
50
0
masl
700
500
0
2 km
MT
C10
C9
C8
C7
C6
C5
C4
C3
C2
C1

709 Fig 9

710

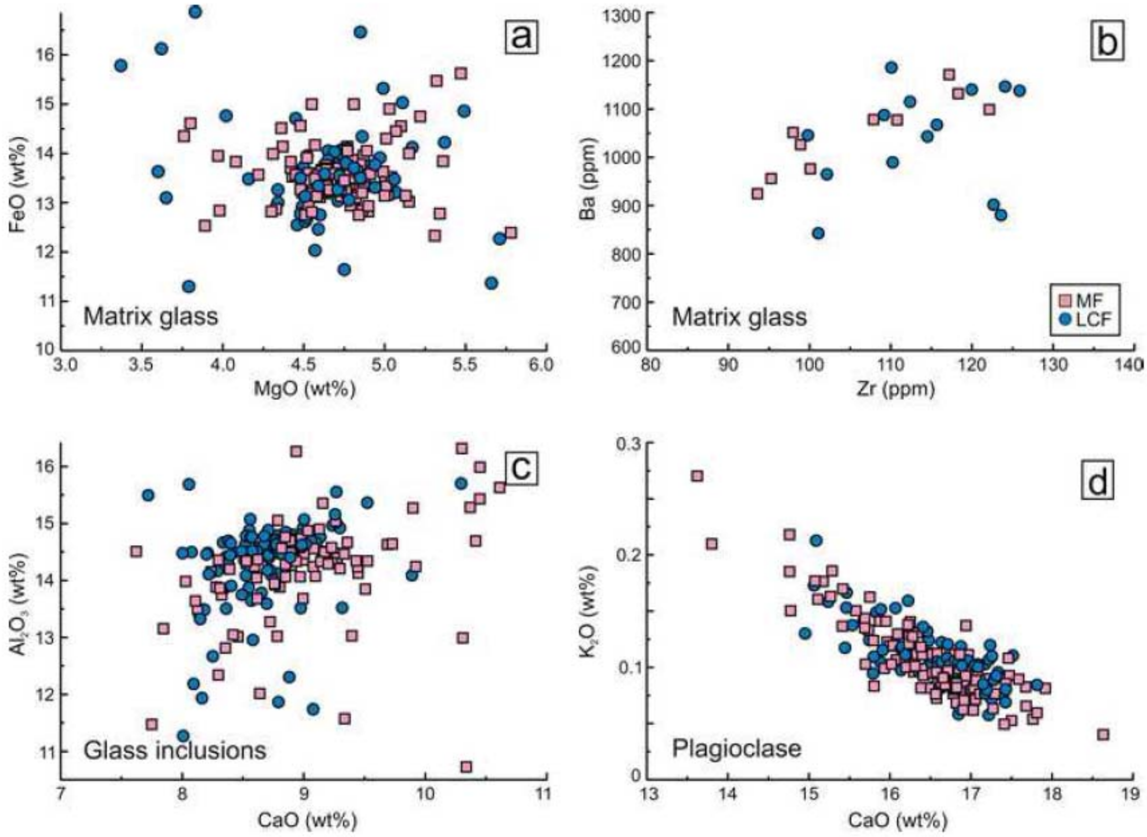

711

712 Fig 10
713

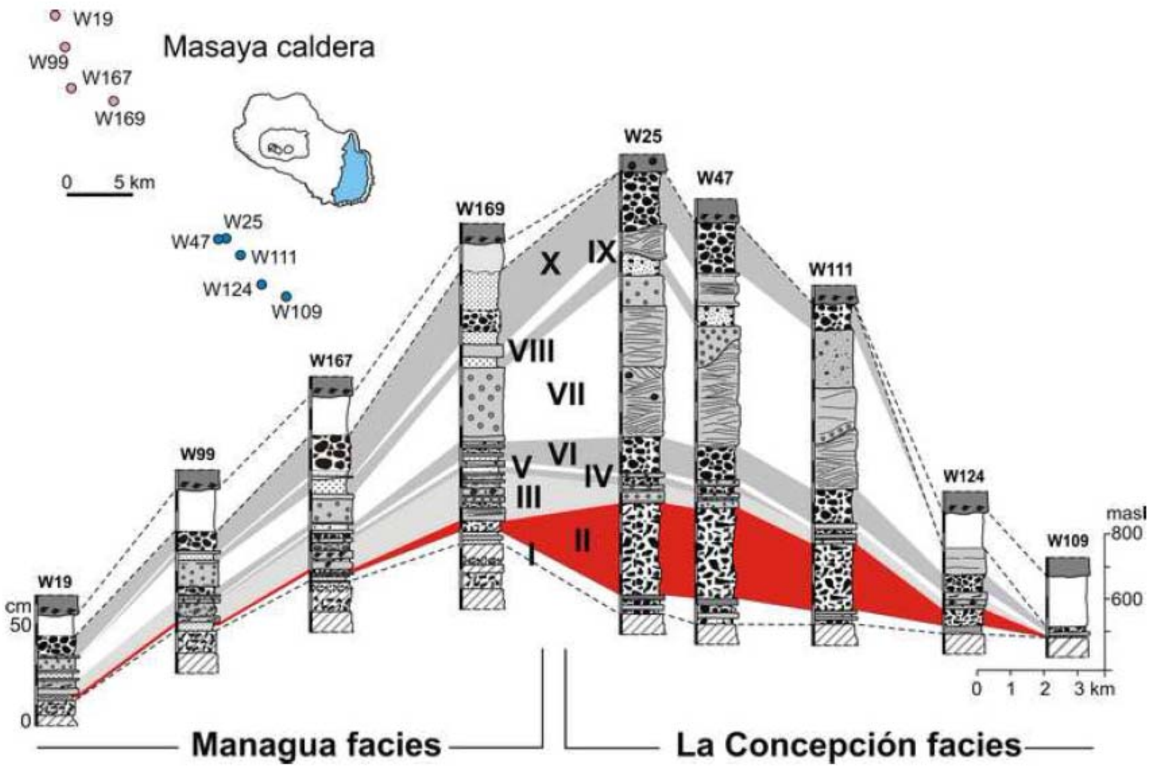

714

Fig 11

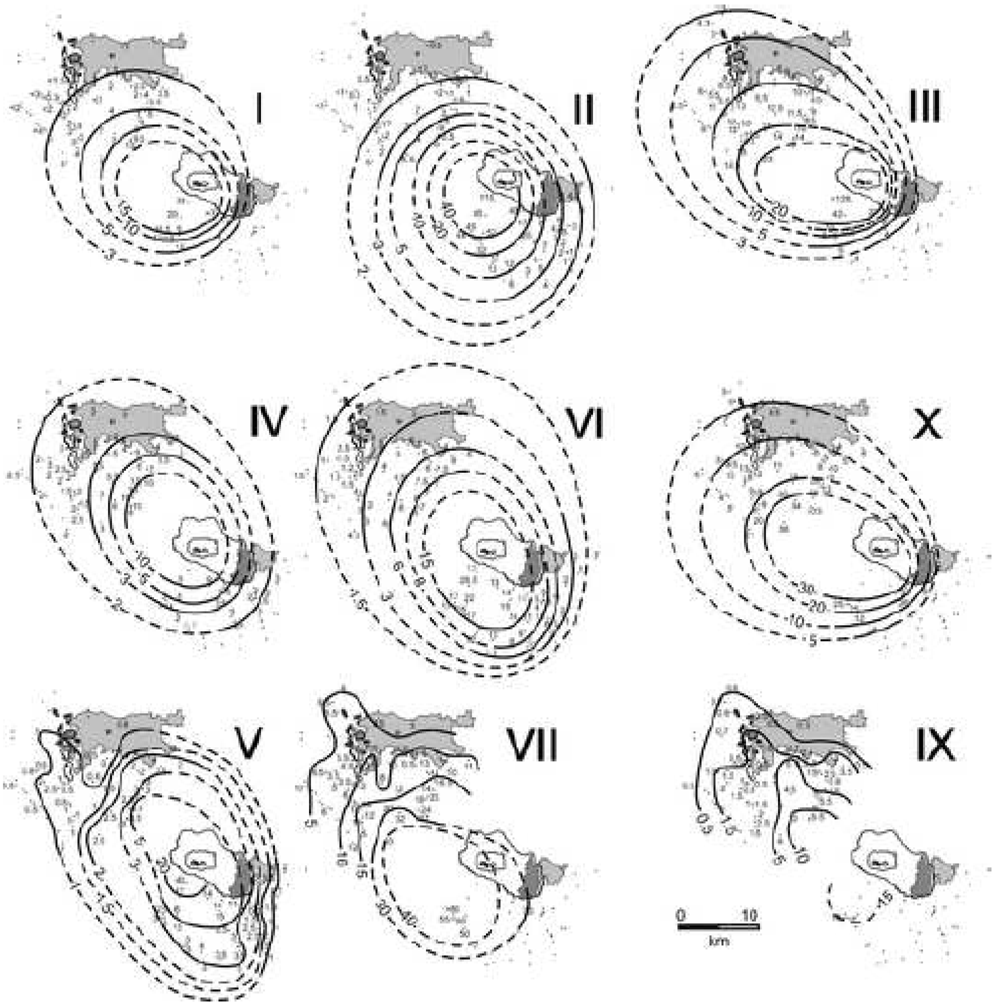

718 Fig 12
719

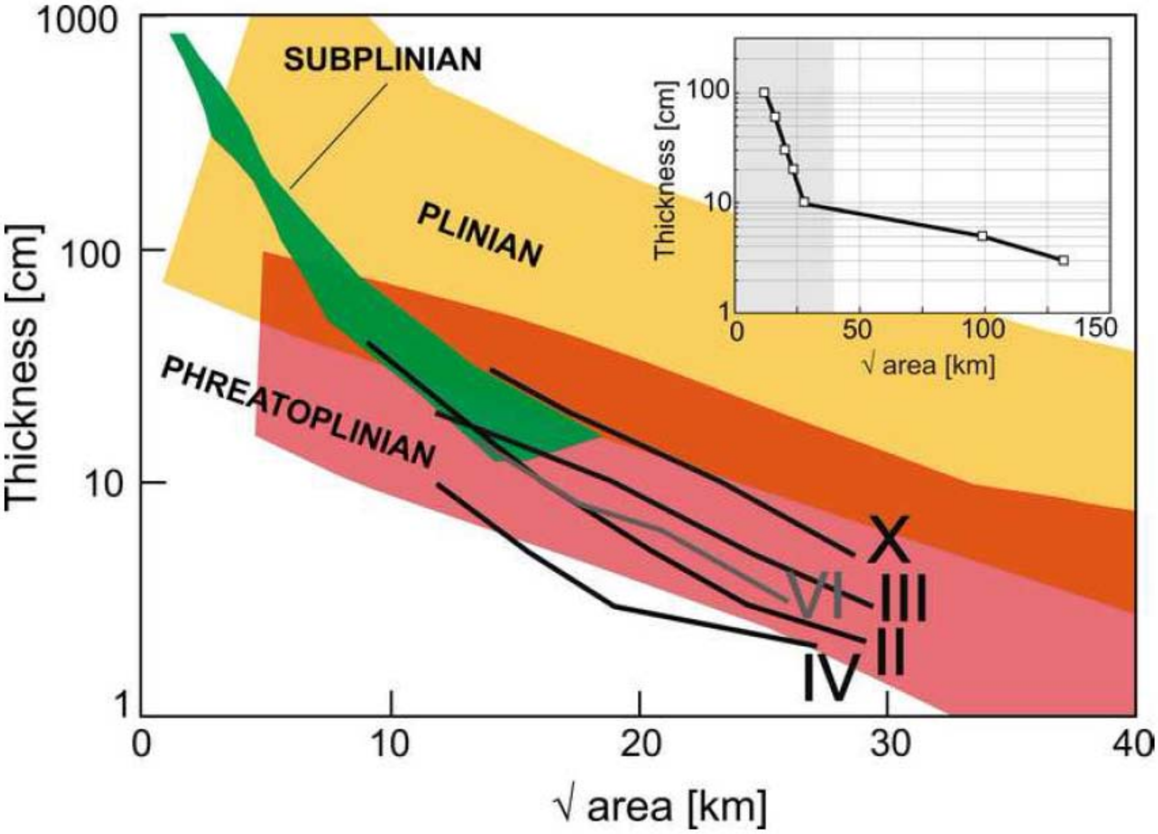

720

721 Fig 13

722

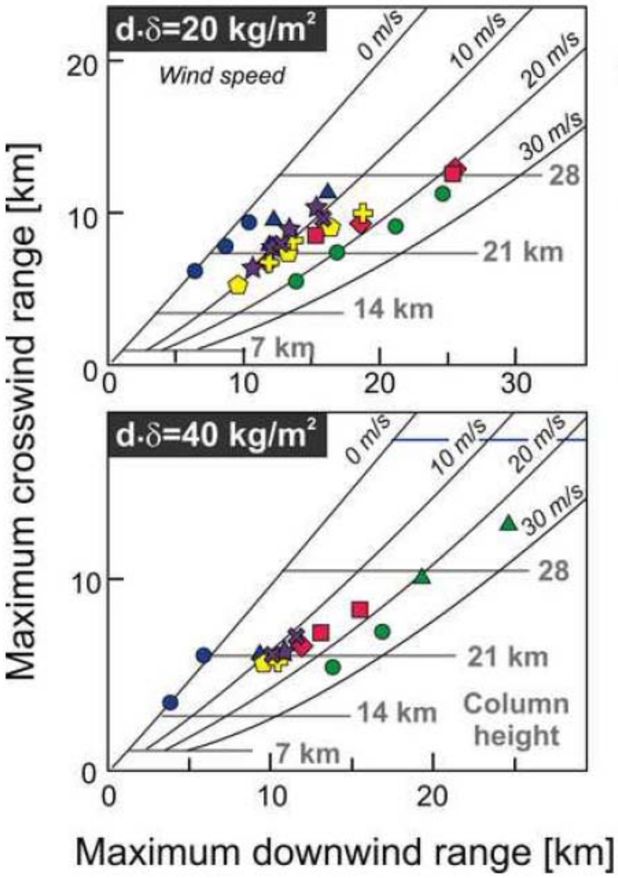

723

Fig 14

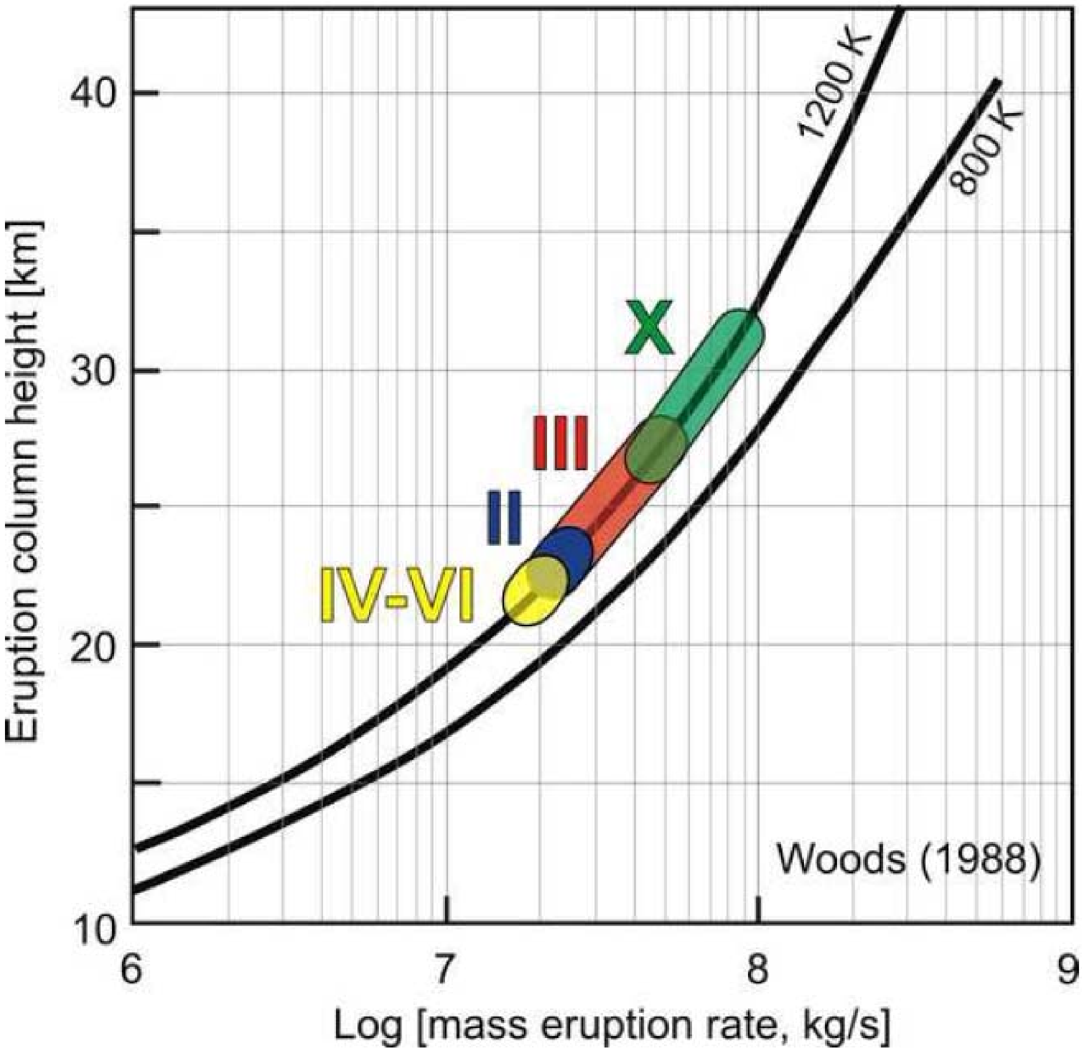
Eruption column height [km]
40
30
20
10
6
7
8
9
Log [mass eruption rate, kg/s]
1200 K
800 K
X
III
II
IV-VI
Woods (1988)

727 Fig 15

728

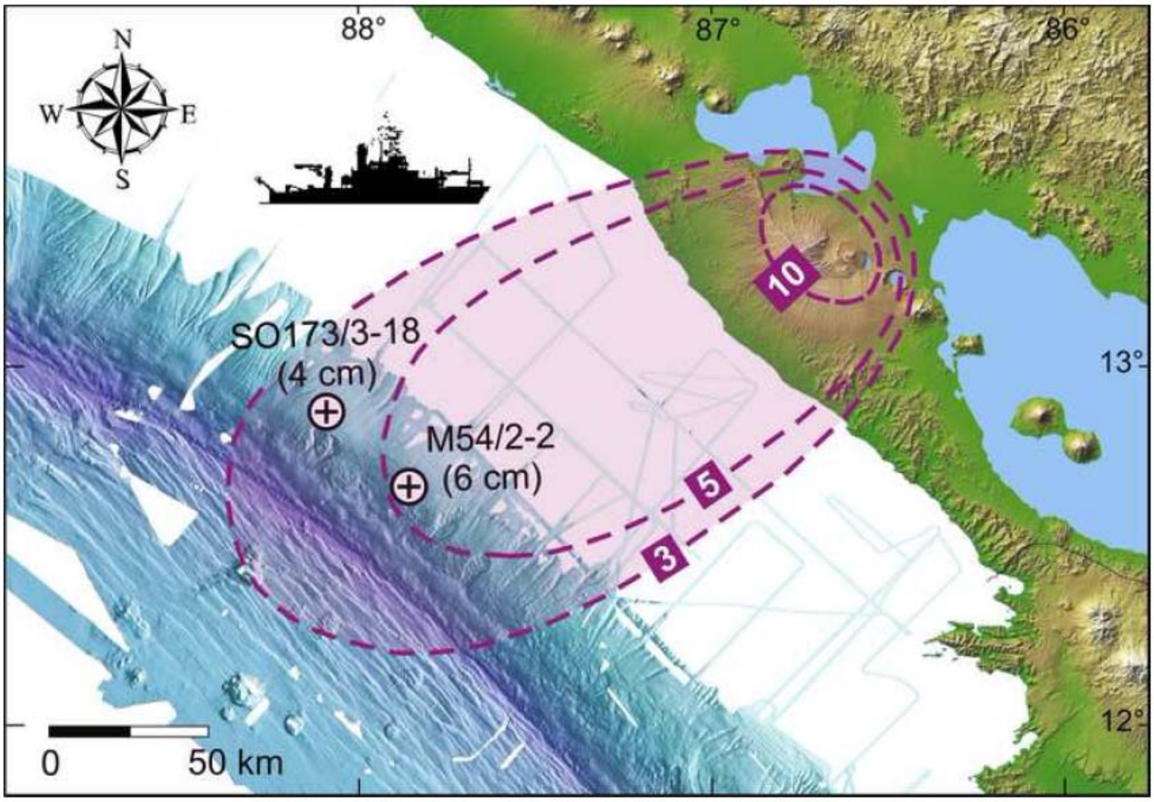

729

Fig 16

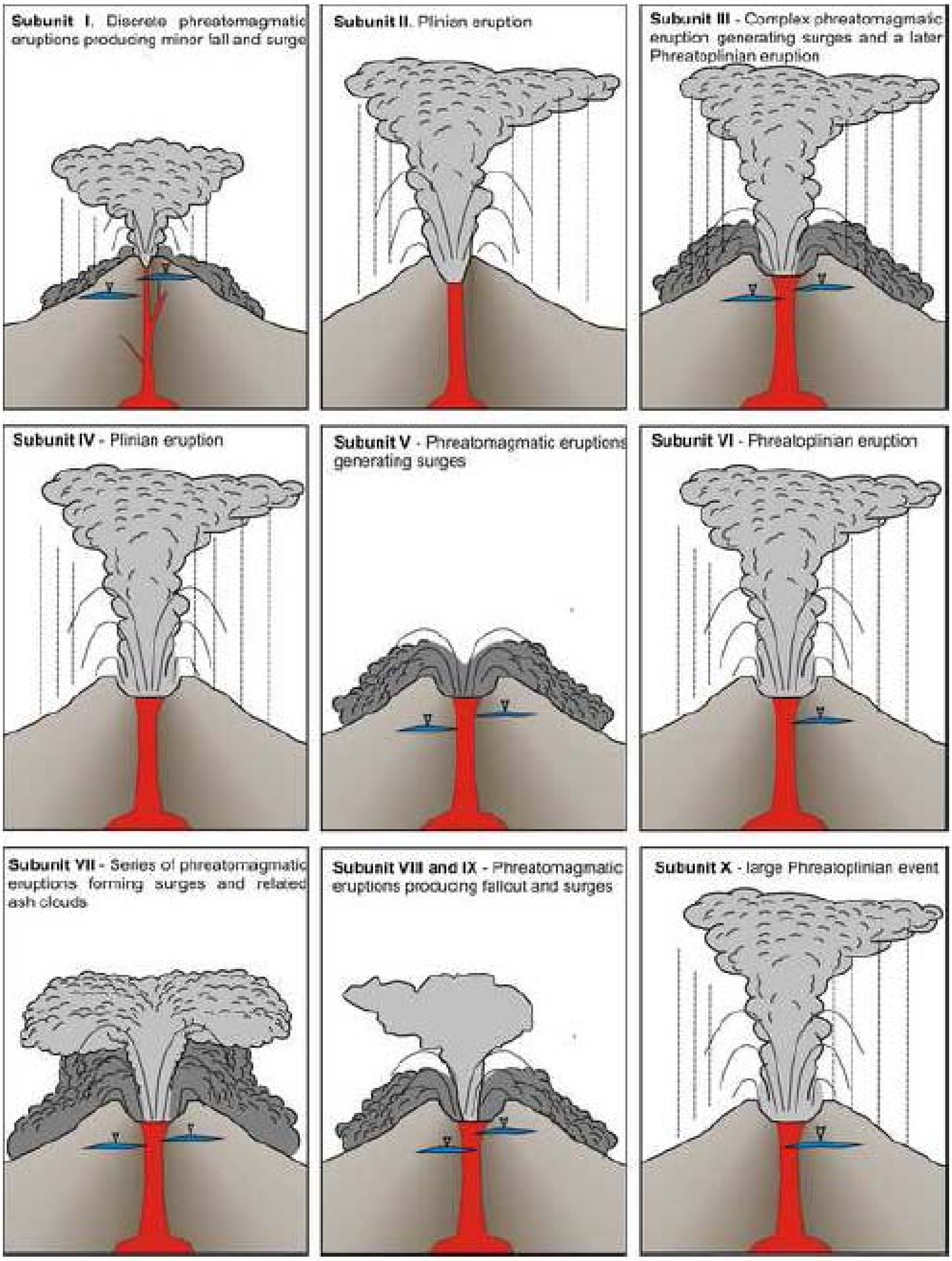
Subunit I. Discrete phreatomagmatic eruptions producing minor fall and surge
Subunit II. Plinian eruption
Subunit III - Complex phreatomagmatic eruption generating surges and a later Phreatoplinian eruption
Subunit IV - Plinian eruption
Subunit V - Phreatomagmatic eruptions generating surges
Subunit VI - Phreatoplinian eruption
Subunit VII - Series of phreatomagmatic eruptions forming surges and related ash clouds
Subunit VIII and IX - Phreatomagmatic eruptions producing fallout and surges
Subunit X - large Phreatoplinian event

Table 1. Characteristics of the subunits of La Concepción facies. Most sorting values were estimated in the field but are supported by selected grain-size analyses. Vesicularity estimated in thin sections and calculated from measured clast bulk densities. ND means "not determined".

Correl. subunit	LCF Subunit	Type of deposit	Sorting	Juvenile fragments	Density (g/cm^3)	Vesicularity (vol.%)	Type of glass	Lithic fragments (vol.%, type)
I	B0	Two basal loose fine ash layers and an indurated tuff at the top with accretionary lapilli and plant remains. Present only in proximal areas						
	B1	Scoria lapilli	σ~1.5	Incipiently to moderately vesicular lapilli, round, bread-crust shaped	0.8-1.35	7-17 40-50	Tachylite	~5 vol.%, hydrothermally altered lavas, plutonics,
	B2	Yellowish faintly laminated indurated fine tuff containing very fine accretionary lapilli and molds of grass leaves						
	B3	Fine scoria lapilli	σ~1.5	Poorly to incipiently vesicular lapilli, round shaped	~1.5	ND	ND	1-2 vol.%, mostly hydrothermally altered
	B4	Laminated weakly-cemented tuff with coarse-ash base to very fine top. Consists mostly of poorly to non-vesicular glass shards and a minor fraction (~3-5 vol.%) of highly vesicular achnelith-shaped fragments. Load structures locally disturb the parallel lamination.						
II	B5	Scoria lapilli	σ~1	Glassy, fluidal-shaped achneliths	0.25-1	45-80	Sideromelane	<<1 vol.%, small, hydrothermally altered
III	B6	Grayish indurated tuff with a fine-grained lower part containing accretionary lapilli and a cross-bedded top of fine lapilli to coarse ash						
	B7	Scoria fine lapilli to coarse ash	σ~1.5-2	Moderately vesicular lapilli, ~5-10 vol.% poorly to incipiently vesicular	0.9-1 ~1.5	50-60	Sideromelane and tachylite	<1 vol.% some hydrothermally altered
	B8	Indurated tuff showing dune structures and cross bedding at proximal facies; accretionary lapilli-rich tuff at medial-distal facies						
IV	B9	Scoria lapilli, some ash coated	σ~1.5	~90 vol.% incipiently vesicular, ~10 vol.% moderately vesicular	1.20-1.35 0.9-1.1	~18 40-44	Sideromelane, tachylite, mingled	~1 vol.% lava, mostly reddish altered
V	B10	Indurated grayish tuff, coarser and showing dunes and cross bedding at proximal areas, at distal is fine-grained with accretionary lapilli						
VI	B11	Scoria lapilli	σ~1.7-2	Moderately - poorly vesicular lapilli, incipiently vesicular lapilli, ~20 vol.% moderately vesicular	~0.8 1.2-1.6 ~0.65	17-20 30-45	Tachylite, minor sideromelane	~3-5 vol.% vesicular lava, plutonics, reddish lithics
VII	B12	Two indurated tuff beds, the lowermost of lapilli and coarse-ash with cross-bedding and dune structures containing plant molds, the upper one is finer-grained (ash) with low-angle cross-bedding. Contains armored lapilli with lava and scoria cores.						
	B13	Grayish accretionary lapilli-rich fine tuff containing dispersed scoria lapilli.						
VIII	B14	Lapilli to coarse ash, faint cross-bedding	σ~2.5	Poorly to moderately vesicular, incipiently vesicular lapilli, coated with fine ash	ND	35-50 ~8	Tachylite	ND
IX	B15	Gray to yellowish indurated fine tuff with scattered accretionary lapilli, cross-bedding and lapilli-rich lenses						
X	B16	Scoria lapilli	σ~2	~80 vol.% moderately vesicular, ~15 vol.% highly vesicular, ~5 vol.% dense	~0.4, 0.6-0.7, 1.1-1.5	20-30	Tachylite	~5 vol.% basaltic lavas, some hydrothermally altered

Table 2. Characteristics of the subunits of the Managua facies. Most sorting values were estimated in the field but are supported by selected grain-size analyses. Vesicularity estimated in thin sections and calculated from measured clast bulk densities. ND means “not determined”.

Correl. subunit	MF Subunit	Type of deposit	Sorting	Juvenile fragments	Density (g/cm^3)	Vesicularity (vol.%)	Type of glass	Lithic fragments (vol.%, type)
I	**C1** **a**	Scoria fine-lapilli to coarse ash	σ~1.5	Highly to moderately vesicular scoria lapilli to coarse ash	0.6-1.1	ND	Sideromelane	<1 vol.%, reddish small lithics
	b	Hardened laminated black to purple ash layer which frequently contains a very thin discontinuous yellowish fine layer rich in plant remains						
II	**C2**	Scoria fine-lapilli	σ~1-1.3	Moderately to highly vesicular fluidal glassy scoria	~0.6 0.9-1.1	~70 30-40	Sideromelane	<1 vol.%
III	**C3**	Normal-graded scoria lapilli layer with 30 vol.% of ash, sandwiched by thin tuffs	σ~2-2.5	Mostly round poorly vesicular scoria, minor moderately to poorly vesicular scoria lapilli, mostly coated with fine ash	1.8-2.3 ~1.3	<40 45-65	Mixture of sideromelane and tachylite	~5-15 vol.%, angular aphyric hydrothermally altered lava
IV	**C4**	Slightly normal-graded scoria lapilli layer	σ~1.5	Highly vesicular scoria and minor denser juveniles	0.6-0.8 ~1.3	40-50	Tachylite and lesser vesicular sideromelane	<3 vol.%, basaltic lava fragments
V	**C5**	Indurated yellowish thin tuff, with desiccation cracks at the top and showing a lower cross-bedded portion and leaf molds at proximal outcrops						
VI	**C6**	Scoria lapilli	σ~1.8-2	Mostly highly vesicular glassy light scoria lapilli, but also moderately vesicular and dense	0.6-0.9 ~1.3	10-40	Tachylite, sideromelane at the rims	<5 vol.%, mostly hydrothermally altered
VII	**C7**	Thick yellowish tuff with abundant accretionary lapilli and crude internal stratification, massive or planar bedded						
VIII	**C8**	Coarse ash and few lapilli	σ~2.2	Moderately to poorly vesicular fine lapilli and dense coarse to fine ash	0.7-1.1	>12	Tachylite, minor sideromelane	~2 vol.%, hydrothermally altered fragments
IX	**C9**	Indurated fine tuff with accretionary lapilli and small floating lapilli fragments, at the top a thin hardened level with desiccation cracks						
X	**C10**	Reverse-graded scoria lapilli	σ~1.8-2	Moderately to poorly vesicular lapilli and small fraction of highly vesicular scoria lapilli	1.3-1.7 0.8-0.9	30-60	Tachylite, minor sideromelane	~5 vol.%, mostly hydrothermally altered basaltic lava

Table 3. Volume and eruption parameters calculated for the subunits I-X

Subunit	Volume (km^3)		Column height (km)	Wind speed (m/s)	Mass flux (kg/s)
	Bulk	DRE			
I	0.068	0.028			
II	0.115	0.038	~22-24	<2	10^7-10^8
III	0.125	0.102	~22-28	~10	10^6-10^7
IV	0.052	0.025	~21-23	~10	10^6-10^7
V	0.037	0.015			
VI	0.099	0.038	~21-23	~10	10^6-10^7
VII	0.018	0.007			
VIII	0.076	0.030			
IX	0.046	0.018			
X	0.219	0.115	~26-32	~20	10^6-10^7